

A tourmaline-andalusite-garnet bearing leucogranite within the Monotonous Series, Southern Bohemian Massif, Austria

RICHARD GÖD* & THEODOROS NTAFLOS*

9 Text-Figures, 8 Tables

Österreichische Karte 1:50.000

BMN / UTM

36 Ottenschlag / NM 33-11-16 Ottenschlag

Moldanubicum
Monotonous Series
Leucogranite
Tourmaline
Andalusite
Garnet

Contents

Abstract	57
Zusammenfassung	58
Introduction	58
Regional Geology	58
Local Geology	58
Petrography	58
Macroscopic observations	58
Microscopic observations	59
Sampling and analytical methods	61
Analytical results	61
Whole rock chemistry and trace elements	61
Mineral analyses	62
Feldspars	62
Tourmaline	62
Garnet	63
Andalusite	63
Micas	64
Discussion	64
Conclusions	66
Acknowledgements	66
References	66
Appendix (Tables 2–8)	68

Abstract

The Bernreith leucogranite, embedded within paragneisses of the Monotonous Serie (= Ostrong Unit), is a peraluminous muscovite-tourmaline-andalusite-garnet bearing plutonic body with a primary, magmatic texture. It is characterised by an ubiquitous disseminated tourmaline (schorl) mineralisation and, consequently, by significant boron contents up to 1,300 ppm. An accessory andalusite mineralisation, interpreted as of magmatic origin as well as the occurrence of garnet emphasise the peraluminous chemistry of the Bernreith leucogranite. Low K/Rb ratios ranging between 67 and 136 (with a maximum of 214), a single fluorine content of \approx 2,300 ppm and elevated tin concentrations between 15 and 55 ppm point to a moderate geochemical differentiation within the leucogranitic body. Mineralogical, geochemical and geological similarities between the Bernreith leucogranite and the so called "Blaník orthogneiss[es]" in the Czech part of the Moldanubicum (BREITER et al., 2005; RENÉ & FINGER, 2016) are in favour of grouping them together. The magmatic event giving rise to the formation of the leucogranitic Blaník Orthogneiss[es] is interpreted as an early Paleozoic age (*ibidem*). The Bernreith leucogranite might therefore also, based on the similarities as mentioned, be interpreted as an early Paleozoic age. However, the nature of emplacement of the Bernreith leucogranite as such remains an open question. The lack of an intrusive contact and the lack of any other contact phenomenon seems to be in favour of a tectonic rather than an intrusive interpretation for its emplacement.

* RICHARD GÖD, THEODOROS NTAFLOS: University of Vienna, Department of Lithospheric Research, Josef-Holaubek-Platz 2, 1090 Wien. richard.goed@univie.ac.at, theodoros.ntaflos@univie.ac.at

Ein Turmalin-Andalusit-Granat führender Leukogranit innerhalb der Monotonen Serie, Südliche Böhmischa Masse, Österreich

Zusammenfassung

Der Bernreith Leukogranit repräsentiert einen peraluminösen, Muskovit-Turmalin-Andalusit-Granat führenden plutonischen Körper mit magmatischem Gefüge. Er ist von Paragneisen der Monotonen Serie („Ostrong Einheit“) umgeben. Die disseminierte Turmalinführung (Schörl) ist über den gesamten Leukogranit homogen verteilt. Der als magmatisch interpretierte Andalusit wie auch das Auftreten von Granat unterstreichen dessen peraluminösen Chemismus. Geochemisch sind der hohe Borgehalt (max. 1.300 ppm), leicht erhöhte Zinngehalte (15–55 ppm), niedrige Kalium/Rubidium Quotienten zwischen 67 und 136 (max. 214) sowie ein singulärer Fluorgehalt von 2.300 ppm Zeichen einer moderaten Differentiation.

Zwischen dem Leukogranit von Bernreith und dem sogenannten „Blaník Orthogneis“ (BREITER et al., 2005; RENÉ & FINGER, 2016) innerhalb des tschechischen Anteils der Monotonen Serie bestehen deutliche geologische, mineralogische und geochemische Ähnlichkeiten. Das Alter der „Blaník Orthogneise“ wird als altpaläozoisch angenommen (*ibidem*), was auf Grund der beschriebenen Ähnlichkeiten zum Leukogranit von Bernreith für diesen ebenfalls anzunehmen ist. Die Platznahme des Leukogranites von Bernreith bleibt eine offene Frage. Da weder ein Primärkontakt noch Kontaktphänomene s.l. zu den umgebenden Paragneisen zu beobachten sind, scheint ein tektonischer Kontakt gegenüber einer intrusiven Platznahme des Leukogranites jedoch wahrscheinlicher zu sein.

Introduction

A leucogranite displaying a disseminated tourmaline mineralisation has been found next to the tiny village Bernreith, 3 km NW of Ottenschlag and around 100 km NW of Vienna. The tourmaline mineralisation can be traced for about 1.5 km over the entire length of the granitic body. The tourmaline is associated with accessory andalusite and garnet. The granite is hosted by medium to high grade metamorphic paragneisses but does hardly show any metamorphic overprint still keeping its equigranular, granitic texture. A group of similar tourmaline and sillimanite bearing orthogneisses to “metagranites” have been described from the Czech part of the Moldanubicum and are interpreted as products of an extensive lower Paleozoic magmatic event (BREITER et al., 2005; RENÉ & FINGER, 2016). However, such leucogranites were unknown to date within the Monotonous Series of the Southern Bohemian Massif. This paper aims to describe and classify this rock petrographically and mineralogically.

Regional Geology

The investigated area (Text-Fig. 1) belongs to the Moldanubicum, a significant part of the Bohemian Massif, which in turn is part of the Variscan basement of Europe’s geology. The stratigraphic deepest part of the Moldanubicum, the “Monotonous Series” (also termed as “Ostrong Unit”), is predominantly composed of cordierite bearing as well as cordierite free monotonous paragneisses. Subordinated orthogneisses, scarce calcsilicate gneisses, quartzites and eclogite-amphibolites form additional strata within the paragneisses. For the regional geology, see map sheet 1:50,000, ÖK 36 Ottenschlag (FUCHS, 1979; FUCHS, 1983; FUCHS & FUCHS, 1986; FUCHS & ROETZEL, 1990). Detailed petrological investigations regarding these paragneisses have been carried out (LINNER, 1992, 1996; PETRAKAKIS, 1997; KLÖTZLI et al., 1999) and may be, based on these papers, summarized as follows: an early metamorphic stage is preserved as kyanite-staurolite relics, followed by a peak metamorphism triggering the partial melting, indicating P-T conditions of $720^{\circ} \pm 30^{\circ}\text{C}$ and $P_{\min} = 4.4 \pm 0.4 \text{ kbar}$. Final rehydration reactions recorded by white mica porphyroblasts were estimated with $650\text{--}700^{\circ}\text{C}$ and $3\text{--}5 \text{ kbar}$. Recent zircon dating of an orthogneiss (“Laimbach gneiss”) within the paragneisses in Lower Austria

yielded an age of 475 Ma, revealing at the same time a Cambrian to Ordovician minimum sedimentation age for the paragneisses (STOCKINGER, 2021).

Local Geology

Due to the total cover of the area by meadows, marshy soil and alluvial strata all observations are based on boulders. However, the peneplain of the area investigated, undulating around 700 m a.s.l., excludes significant transport and suggests the boulders to be sub-autochthonous.

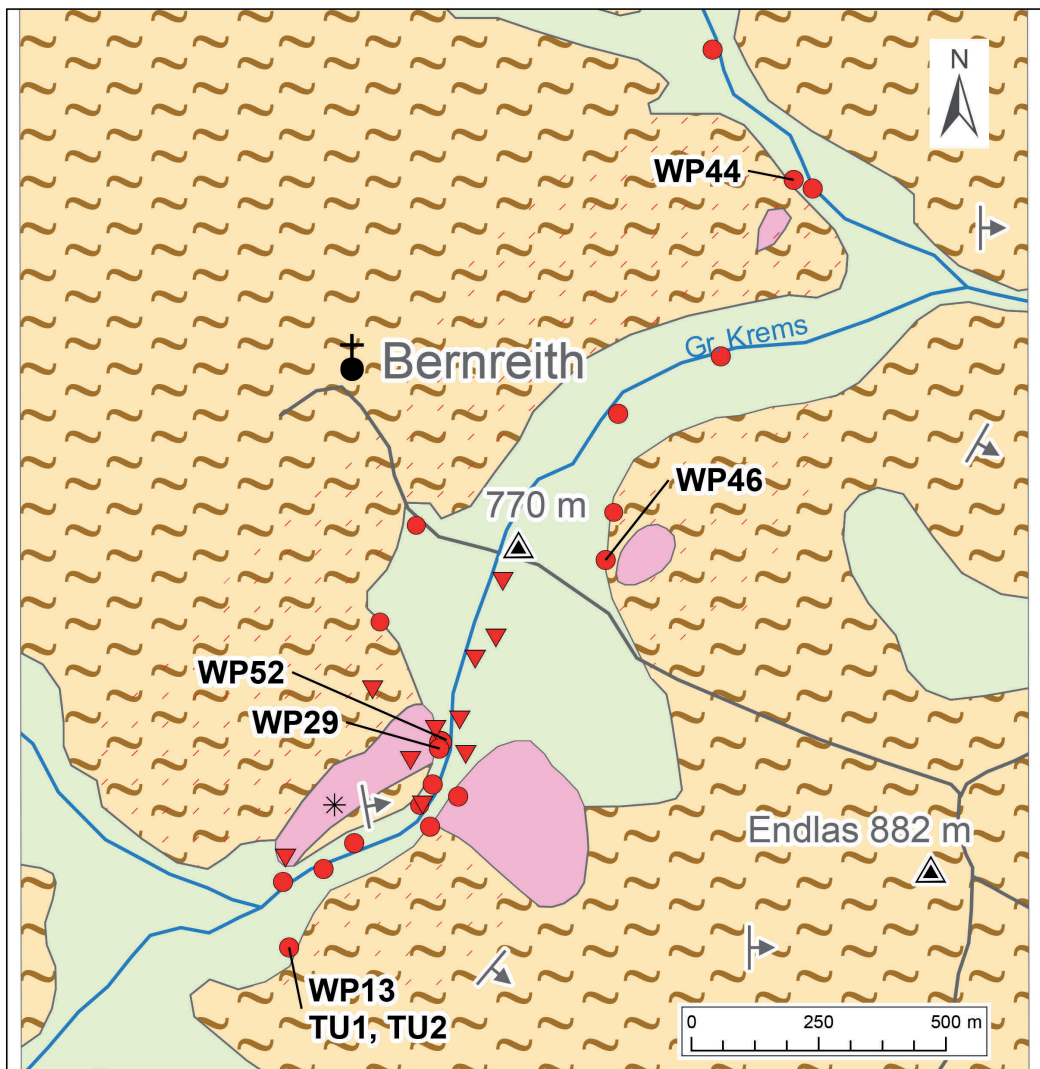
The isolated leucogranitic bodies around the tiny village Bernreith as mapped by FUCHS & FUCHS (1986), confirm a SW-NE extension of the granite around 1.5 km. Remapping suggests a larger extension of the granitic body as shown in the map. The tourmaline mineralisation, locally already mentioned by FUCHS (1979), represents an ubiquitous disseminated mineralisation along the entire extension of the granite.

The granite is hosted by paragneisses as described above. These paragneisses host themselves veinlets of aplites and small, tourmaline bearing pegmatoids. No primary contact between the leucogranite and the paragneisses have been found. A single, doubtless tectonic contact between the leucogranite and the paragneisses occurs south of sample site WP 29 (Text-Fig. 1). It is made up by a lit parlit, 12 m thick sequence of alternating granite and paragneiss lamellae varying between dm to m in thickness. The lamellae strike $\approx \text{N-S}$ and dip $\approx 70^{\circ} \text{ E}$, almost perpendicular to the general orientation of the granitic body.

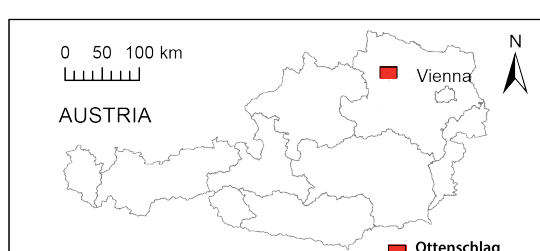
Petrography

Macroscopic observations

The leucogranite displays an overall homogeneous, equigranular texture without any preferred orientation. However, a very weak lineation may occur locally. Two subtypes can be distinguished, a coarse grained one with average grain sizes around 5 mm and a fine grained variety with grain sizes around 1 mm to 2 mm. Due to the lack of outcrops, their spatial and volumetric relation cannot even be estimated. Quartz, milky feldspars and tourmaline is the dominating paragenesis across the whole extension



Text-Fig. 1.
Local geology around the village Bernreith after FUCHS & FUCHS (1986); detail from Geological Map of Austria 1:50,000, sheet 36 Ottenschlag, Geological Survey of Austria, Vienna; remapped and modified.

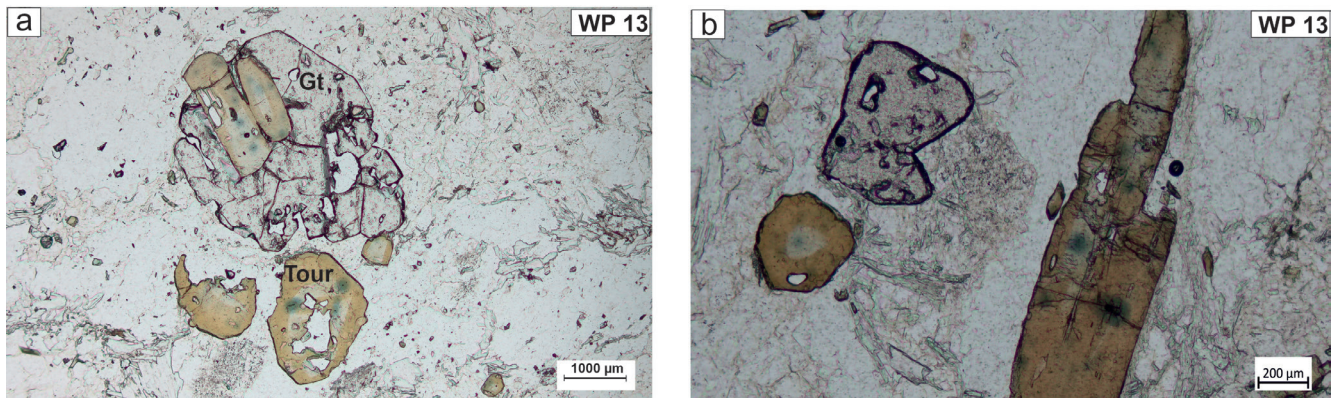


Alluvial sediments
Leucogranite
Paragneiss
Small aplitic and pegmatitic lenses
Sub-autochthonous granitic boulders
● Tourmaline macroscopically visible
▼ Tourmaline macroscopically not visible
↗ Strike/dip direction
WP29 Sample number
* Tectonic contact

of the granitic body. While the disseminated tourmaline in the coarse grained subtype tends to form xenomorphic "patches" of ~ 5 mm in diameter, the tourmaline in the fine grained variety forms thin needles up to a (rare) maximum length of close to 10 mm. They contribute to an estimated volume of around 1 Vol.-% to the granite. Rare pegmatitic schlieren up to 20 cm in size, containing tourmaline crystals of a few cm length, occur locally within the granite. Muscovite content is always below 1 Vol.-% and rarely exceeds grain sizes of 1 mm. Small garnets of around 1 mm in size are occasionally visible by naked eye (e.g. sample WP13). Biotite is even scarcer and seems to be restricted to the coarse-grained subtype of the granite.

Microscopic observations

A total of 15 thin sections have been investigated. A striking general feature is the typical magmatic texture and the absence of foliation. All of them mirror the non-foliated, primary granitic texture as described. Quartz forms mostly a fine grained, somewhat "fluidal" matrix between the significantly larger feldspar individuals. Microcline grains are xenomorphic to hypidiomorphic, perthitic and in the average smaller than the plagioclase grains. No myrmekitic intergrowths have been observed. The plagioclases are mainly hypidiomorphic, weakly zoned and almost completely sericitised. Some of them bear quartz inclusions.



Text-Fig. 2.

- a) Coexisting garnet and tourmaline. Tourmaline with pleochroitic halos (blueish colour) around the zircon inclusions.
- b) Zoned tourmaline with homogeneous core also with pleochroitic halos around zircons.

Tourmaline is homogeneously distributed across the granitic body, displaying a hypidiomorphic to idiomorphic shape. The crystals show a blue-coloured core surrounded by a brownish coloured rim and include numerous extremely tiny zircons triggering pleochroitic halos of some few 10 μ in diameter (Text-Figs. 2a, b).

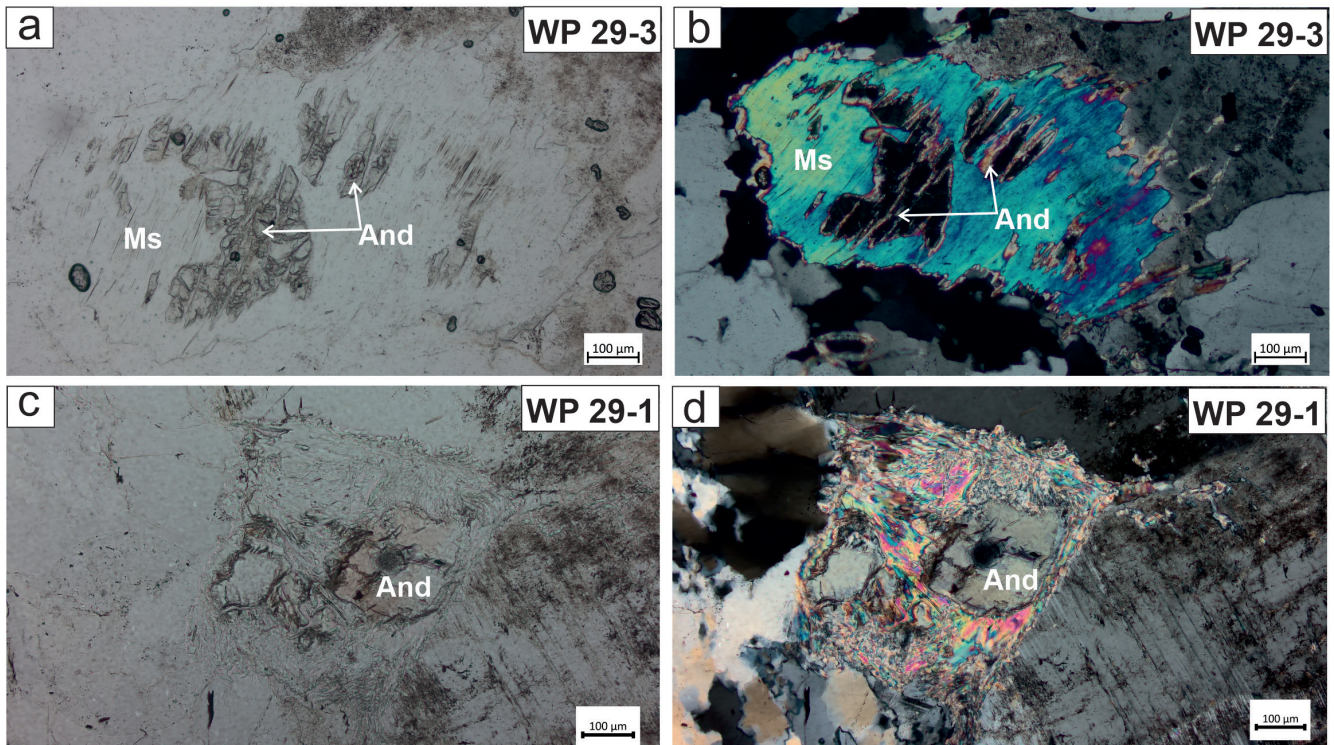
A significant accessory mineral occurring in both subtypes is andalusite, predominantly ranging in size between $\approx 200 \mu$ and $\approx 400 \mu$. All the grains are xenomorphic and surrounded by polycrystalline aggregates or single muscovite individuals. These alterations may ultimately replace the andalusite to various degrees (Text-Figs. 3a-d).

Various kinds of muscovite can be distinguished: a) rare, tiny individuals within the granitic matrix, sometimes of a weak, pale-green colour. These muscovites are interpret-

ed as of primary magmatic origin; b) fibrous aggregates of lately formed muscovite, mainly along grain boundaries of feldspars; c) muscovite as product of sericitisation of plagioclases; d) muscovite as alteration product of andalusite.

Hypidiomorphic to skeletal shaped small garnets with average grain sizes below 1 mm occur as rare accessory mineral across the granite. The garnets are free of inclusions. They may be intergrown with tourmaline (Text-Figs. 2a, b).

Biotite is extremely rare and absent in most of the thin sections. Apatite is likewise a rare accessory mineral; no zircons other than those included in tourmalines have been found.



Text-Fig. 3.

- Relictic, partially replaced andalusite surrounded by mostly fibrous muscovite crystals (a, c: PPL; b, d: XPL); andalusite is characterised by a slightly rose colour in 3c.

Sampling and analytical methods

Due to the complete lack of outcrops, sampling focused exclusively on sub-autochthonous boulders, reaching average sizes of some few meters in diameter. Therefore, sampling had to be carried out using a portable “petrol drill and breaker” device. In this study, 15 thin sections have been prepared for petrographic description and 5 polished thin section for electron microprobe analyses. Sample sizes for chemical analyses were in the order of 3 kg each. The samples were comminuted via jaw crusher, split and ground using an agate mill. The whole rock major and trace elements were performed on a sequential X-Ray spectrometer PHILIPS PW2404 using a super-sharp endwindow tube with a Rh-anode and a programmable 4 kW generator (60 kV max., 125 mA.; iso-Watt-switching), the accompanying software is PANalytical “SuperQ” vers. 5.1B (5.2822.3). Major elements were determined on calcined rock powder fused with lithium tetraborate as flux to form a glass bead. Trace elements were determined directly on the crushed and milled rock powder mixed with poly-vinyl alcohol as a binding agent to form a pressed powder pellet. These analyses have been carried out at the Department of Lithospheric Research, University of Vienna. Fluorine and boron have been analysed by a commercial laboratory: fluorine by KOH fusion and an ion selective electrode and boron by NaOH fusion and ICP-MS finish.

Mineral analyses were carried out with a Cameca SXFive FE Electron Probe Microanalyzer (EPMA) at the Department of Lithospheric Research, University of Vienna. All analyses were performed against natural and synthetic standards by utilizing wavelength-dispersive spectrometers. The acceleration voltage, the beam current and the counting time on the peak position were 15 kV, 20 nA and 20 seconds respectively, and standard correction procedures were applied. For the feldspars, in order to avoid loss of the alkalies Na and K, a 5 µm in diameter defocused beam current and 10 seconds counting time on peak position were applied.

The identification of the Al_2SiO_5 polymorph as andalusite were made via Raman spectroscopy. This was done by using a Horiba LabRAM HR Evolution system equipped with Olympus BX-series optical microscope, 1,800 grooves per mm diffraction grating, and Peltier-cooled, Si-based charge-coupled device detector. The spectrum was excited with the 633 nm emission of a He-Ne laser (10 mW). A 100' objective (numerical aperture 0.90) was used to focus the light onto the sample surface. More experimental details are described elsewhere (ZEUG et al., 2018).

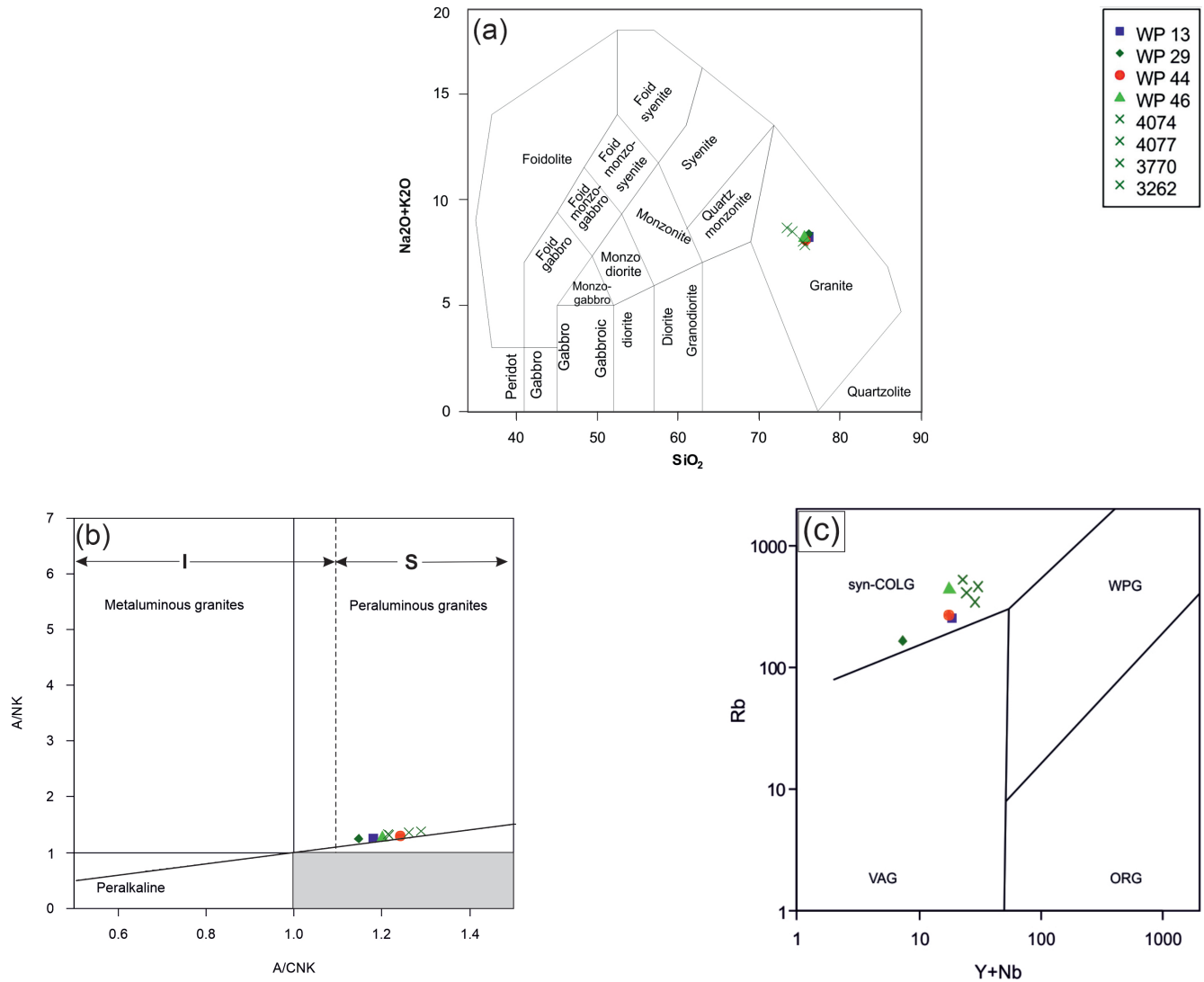
Analytical results

Whole rock chemistry and trace elements

Four samples have been analysed for their bulk and trace element chemistry (Tab. 1). The samples WP 13, WP 44 and WP 46 correspond to the fine-grained subtype whereas sample WP 29 represents the coarse-grained subtype. The bulk composition is consistent with the chemistry of a leucocratic granite, displaying SiO_2 contents around 74.0 wt-%, low iron, magnesium, and calcium contents and an alkali-content (Na_2O plus K_2O) of ≈ 8.0 wt-% (Text-Fig. 4a). The fine-grained subtype displays K/Rb ratios of

Sample	WP 13	WP 29	WP 44	WP 46
SiO_2	75.32	74.80	74.26	74.34
TiO_2	0.06	0.07	0.07	0.04
Al_2O_3	13.88	13.82	14.21	14.24
$\text{Fe}_{2\text{O}}_3^{\text{T}}$	0.65	0.42	0.78	0.74
MnO	0.08	0.02	0.08	0.09
MgO	0.10	0.10	0.08	0.06
CaO	0.40	0.52	0.34	0.34
Na_2O	3.99	3.93	3.99	4.50
K_2O	4.13	4.28	3.94	3.54
P_2O_5	0.32	0.27	0.32	0.44
LOI	0.49	0.43	0.62	0.50
SUM	99.42	98.67	98.69	98.83
<hr/>				
K/Na	1.16	1.22	1.1	0.98
K/Rb	136	214	120	67
Rb/Sr	8.1	3.2	34	29
Al/CNK	1.18	1.16	1.24	1.2
<hr/>				
F	2,350	350	730	790
B	1,020	1,120	1,010	1,330
Ba	63	102	20	25
Rb	252	166	272	437
Sr	31	52	8	15
La	1.7	1.4	2.2	0.94
Ce	5	< 1	6	5
Y	10	3	6	6
As	4	2	2	11
Pb	23	30	13	10
Zn	28	18	38	38
Cu	7	8	7	7
Mo	< 1	< 1	< 1	< 1
Cs	26	10	27	70
Li	121	32	24	45
Be	4	1.2	0.8	2.2
Sn	25	15	32	55
W	10	3	6	6
Nb	8.7	4.4	14.7	11.7
Ta	< 1	< 1	2	3
Th	0.5	0.3	0.5	0.3
U	1.6	0.8	1.7	1.8
Zr	20	19	33	22
<hr/>				
Rb/Sr	8.1	3.2	34	29
U/Th	3.2	2.7	3.4	6
† Fe total as $\text{Fe}_{2\text{O}}_3$				

Tab. 1.
Major and trace elements of the leucogranites from Bernreith.



Text-Fig. 4.

a) Total Alkali vs. Silica classification diagram after MIDDLEMOST (1994).

b) Plot of the Bernreith leucogranites in the A/NK vs. A/CNK diagram (NÉDÉLEC & BOUCHEZ, 2015 and references therein), with I- and S-type domains clearly show their peraluminous character.

c) In the discrimination diagram, Rb vs. Y+Nb (PEARCE et al., 1984) the leucogranites plot within the syn-COLG field. VAG: volcanic-arc granites, syn-COLG: syn-collisional granites, WPG: within-plates, ORG: ocean ridge granites.

The samples with the symbol x in the legend are from BREITER et al. (2005).

136, 120 and 67 respectively whereas the K/Rb ratio of the coarse-grained sample WP 29 displays a significant higher ratio of 214. All studied samples plot to the peraluminous field of the A/NK vs. A/CNK diagram with ratios ranging between 1.16 and 1.24 (Text-Fig. 4b).

The trace element composition is dominated by a boron content ranging between 1,010 to 1,330 ppm. The fluorine content varies strongly from 350 to 2,350 ppm. Elevated tin contents ranging between 15 and 55 ppm are noteworthy. The sample WP 46, obviously the most evolved one, displays the highest Rb and Cs content (437 and 70 ppm respectively). Though the absolute concentrations of uranium and thorium are surprisingly low, the ratio U/Th is > 1 . These erratic trace element contents and ratios point again to some moderate internal differentiation as already mentioned. A very low Zr content (19–33 ppm) has to be emphasised as well.

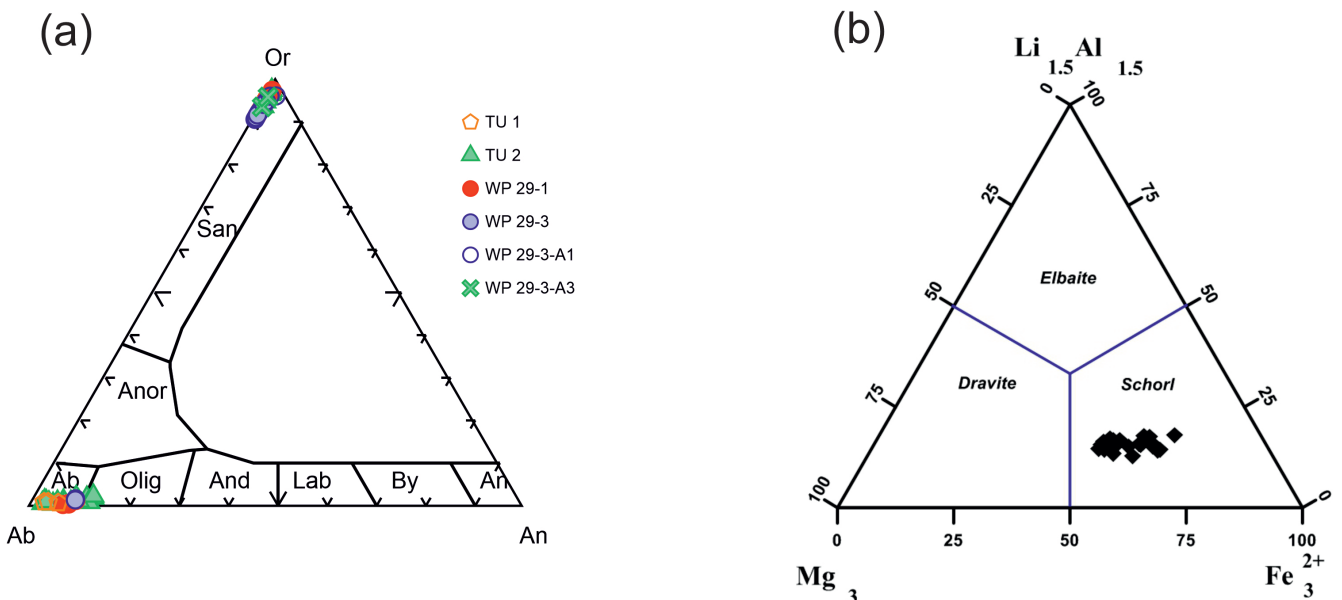
Mineral analyses

Feldspars

The feldspars are albite-rich plagioclases and orthoclase-rich potassium feldspars. No compositional zoning has been observed in both kind of feldspars. The albite components of the potassium feldspars range between 2.5 and 9.4 wt-% (Tab. 2) whereas the anorthite contents of the plagioclases vary between 1.9 and 11.7 wt-% (Tab. 3 and Text-Fig. 5a).

Tourmaline

Tourmaline electron microprobe analyses are given in Tables 4a, b. According to their chemical composition are classified as schorl species (Text-Fig. 5b). BSE image as well as X-Ray elemental maps show an oscillatory zoning with a homogeneous core and slight compositional variations among the concentric zones (Text-Fig. 6). Compared



Text-Fig. 5.
a) Ternary feldspar diagram. The feldspars (Tabs. 2, 3) in the Bernreith leucogranites are closely albites and orthoclase endmembers.
b) Tourmaline ternary classification diagram after HAWTHORNE & HENRY (1999): the tourmaline in the Bernreith leucogranites belongs to the Schörl species (Tab. 4a). The diagram is based on the formula calculation according to YAVUZ et al. (2006).

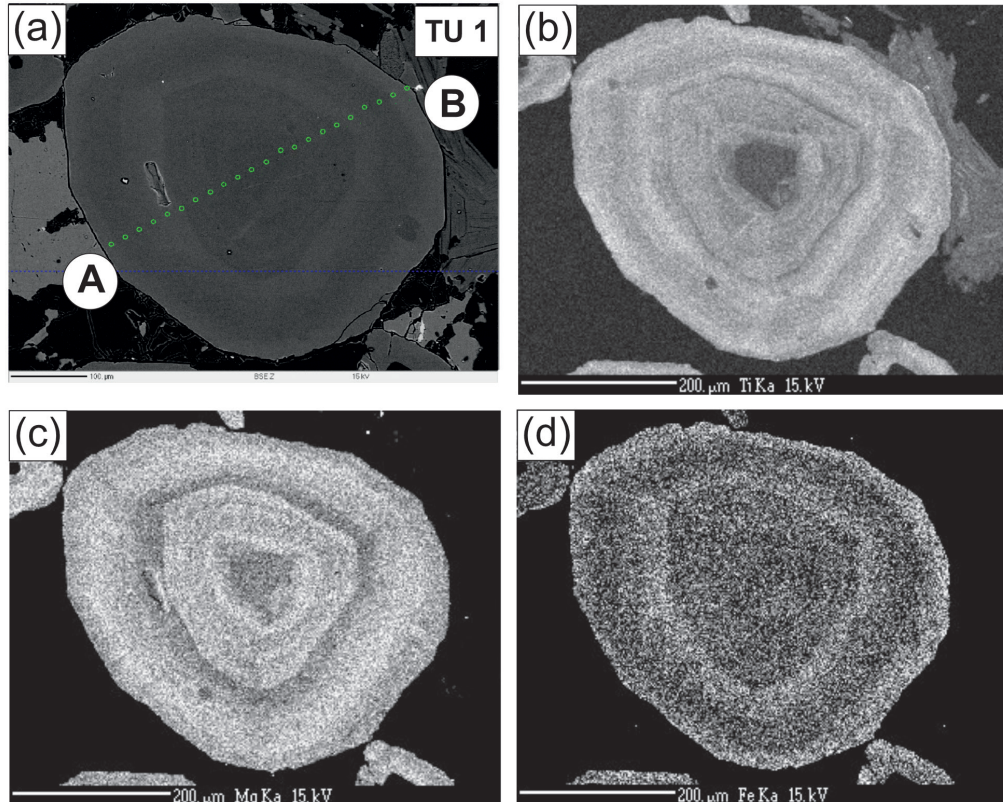
to the rim, the homogeneous core, up to 160 microns wide (Text-Fig. 7), is silica- and alumina-rich ($\text{SiO}_2 = 35.6\text{--}36.0$ and $\text{Al}_2\text{O}_3 = 36.0\text{--}36.2$ wt-%) and lower in Mg, Na,Ca,Ti (average in wt-%, $\text{MgO} = 3.0$, $\text{Na}_2\text{O} = 1.42$, $\text{CaO} = 0.07$, $\text{TiO}_2 = 0.31$). The FeO content varies insignificantly between core and oscillatory zones (average $\text{FeO} = 9.6$ wt-%). The homogeneous core indicates slow crystallization rates while the oscillatory zoning supports a change towards faster crystallization rates.

Garnet

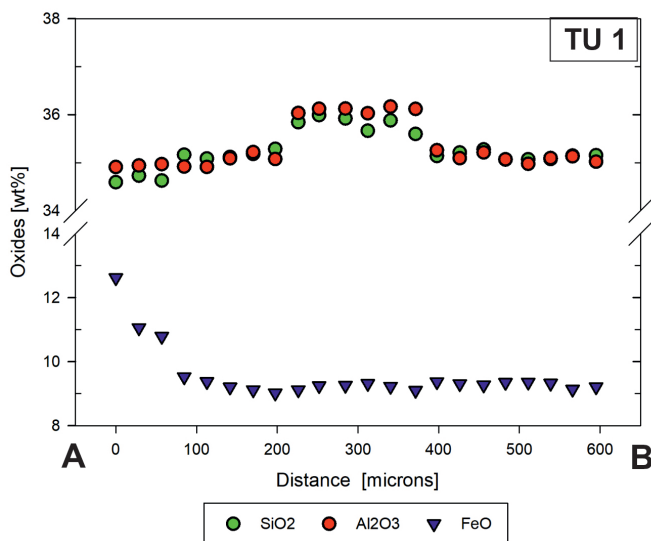
Six individual grains have been analysed, the results are given in Table 5. The almandine component varies between $\approx 51\%$ and $\approx 60\%$, the spessartine between $\approx 38\%$ and $\approx 47\%$ and the pyrope between $\approx 1\%$ and 2% respectively. The grossular and andradite are below 1%.

Andalusite

Andalusite chemical analyses are given in Table 6. The FeO content varies between 0.17 and 0.29 wt-%. Howev-



Text-Fig. 6.
X-Ray elemental maps of Ti, Mg and Fe in tourmaline of the sample TU 1 show a relative homogeneous core followed by variably thick oscillatory zones.
a) Backscattered Electron image (BSE). b) Ti elemental map. c) Mg elemental map. d) Fe elemental map.

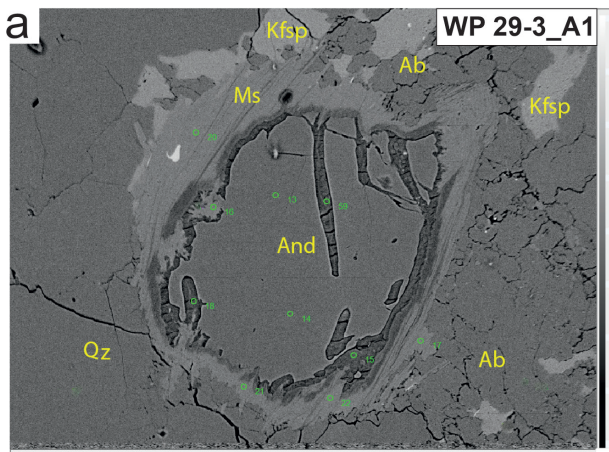


Text-Fig. 7.
Profile A–B of SiO_2 , Al_2O_3 and FeO in wt-% across a tourmaline from sample TU 1 (Text-Fig. 6a).

er, in two grains the FeO content, with an average around 1.0 wt-%, is significantly higher. As shown in Text-Figures 8a and b, reaction rims with a thickness of some few micrometers are developed between the andalusite and the surrounding muscovite. The chemistry of this obvious alteration zone is extremely heterogeneous, displaying highly varying silica, aluminium, iron and magnesium contents. A striking feature, however, is the low potassium content that never exceeds 1.0 wt-%. The microprobe analyses yield a total varying between 82 and 88 wt-% indicating the high but variable amount of H_2O (Tab. 7).

Micas

As described, muscovite occurs disseminated within the matrix as rare, tiny grains, as alteration products along grain boundaries of feldspars and also as alteration products after andalusite. Four grains of matrix hosted muscovites and fifteen muscovites derived from andalusite alteration have been analysed (Text-Fig. 8). The main chemical difference between the matrix related mica and the one resulting from the alteration of andalusite is reflected by their



Text-Fig. 8.

Andalusite alteration products consisting of hydrous Al-rich silicates have been developed around the margin of andalusite. The presence of hydrous Al-rich silicates within andalusite (a) and along cracks (a, b) predates the formation of white mica where both andalusite and alterations are included.

different FeO contents of 1.31 for the matrix related ones and 0.35 wt-% for the alteration related ones. Microprobe analyses of mica are given in Table 8.

Discussion

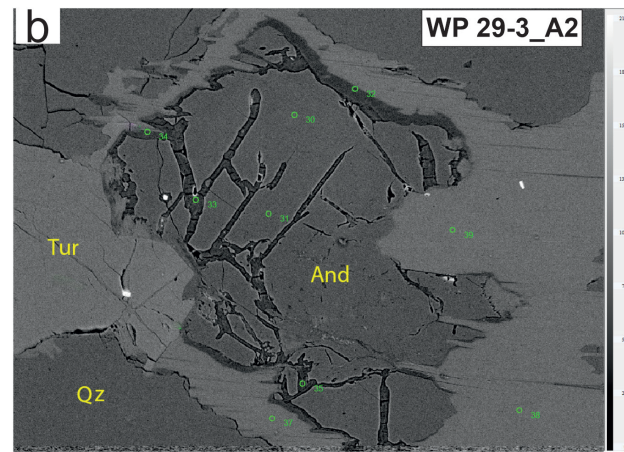
Whole rock analyses from four representative samples along the SW to NE extension (Text-Fig. 1) are given in Table 1. The sample WP 29 refers to the coarse-grained subtype, the samples WP 13, WP 44 and WP 46 refer to the fine-grained subtype. As mentioned, no spatial or voluminous relation between these two subtypes can be established.

The bulk chemistry corresponds to a leucogranite with a peraluminous signature. There is no significant difference between the two subtypes. The bulk chemistry of the leucogranite is of peraluminous character (Text-Fig. 4b) and plots into the field of syncollision granites (Text-Fig. 4c).

A striking feature of the investigated leucogranites is the high boron concentration that varies from 1,000 to 1,300 ppm (Tab. 1).

The fine-grained leucogranites WP 13, WP 44 and WP 46 have K/Rb ratios of 136, 120 and 67 ppm indicating that they have experienced moderate fractional crystallization on their way to solidification. The coarse-grained sample WP 29 has the highest K/Rb ratio of 214 and appears to be less fractionated. This is also emphasized by a U/Th ratio varying between 3.2 and 6.0 and by the slightly elevated Sn contents ranging from 25 to 55 ppm for the fine-grained leucogranites (Tab. 1).

Not all trace elements point to moderate fractional crystallisation. Boron concentrations up to 1,300 ppm are evidently among the highest reported in leucogranites (e.g. PESQUERA et al., 2013; KLOMÍNSKÝ et al., 2010). Apparently, the high boron concentrations are attributed to the disseminated, ubiquitous tourmaline mineralization. Considering the fact that the average B content in the upper continental crust is 17 ppm (RUDNIK & GAO, 2014), it is evident that the origin of the extremely high B contents in the investigated samples could not be explained by melting



of an upper crust with an average composition. Likewise, the moderate fractional crystallization fails to explain the high boron concentration. In case, tourmaline is a dominant phase, biotite might just occur as an accessory mineral or even be absent (PESQUERA et al., 2013) – which is in perfect accordance with the observations as described.

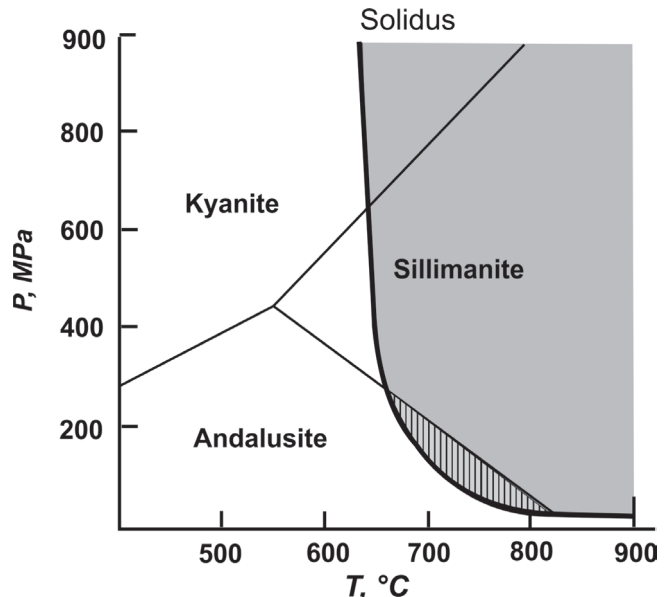
It is well known, that boron rich fluids frequently form aureoles in wall rocks giving rise to some kind of tourmalinisation (e.g. LONDON, 1999). No phenomenon of that kind has been observed. Small, schist parallel “pegmatoids” spatially dispersed around Bernreith within the paragneisses (Text-Fig. 1) seem to be of “small scale” anatexitic origin genetically not associated to the leucogranite.

Andalusite as such is not an uncommon accessory mineral in leucogranites and has been mentioned – also in paragenesis with tourmaline – from the Bohemian Massif elsewhere (BURIANEK & NOVAK, 2001, 2007). As experimentally shown and discussed exhaustively in CLARKE et al. (2005), the aluminosilicate stability field and the water saturated peraluminous granite solidus overlap themselves permitting a magmatic origin for andalusite (Text-Fig. 9). The andalusite is herein therefore interpreted as a primary, magmatic component. Two chemically different kinds of andalusite, separated by iron contents around 0.2 wt-% FeO and around 1 wt-% FeO respectably, have been observed (Tab. 6). However, due to the limited data, no further interpretation is possible.

All andalusite grains are altered in a twofold manner (Text-Figs. 8a, b): each grain is coated by a reaction rim some μ thick, outward followed by fine-grained, radiating muscovite. This muscovite may alter the andalusite partially (in most of the observed cases) or may completely consume the andalusite grain.

The leucogranite is hosted by the medium to high grade metamorphic paragneisses of the “Monotonous Serie” (Ostrong Unit). The leucogranite has, nevertheless, not been affected by a metamorphic event and displays predominantly a homogeneous, equigranular magmatic texture. However, a very weak, locally restricted parallel texture is interpreted as of (late) magmatic origin. No primary contact to the surrounding paragneisses was observed. A unique tectonic contact some meters thick is characterised by a lit par lit sequence of granite and paragneiss (Text-Fig. 1). Assuming a magmatic origin of andalusite, depth and crystallisation temperatures for the leucogranite are restricted on the one hand by the stability field of andalusite and on the other hand by the hydrated solidus line (HOLDAWAY, 1971; CLARKE et al., 2005; PHILPOTTS & AGUE, 2009; NEDELEC & BOUCHEZ, 2015; see also Text-Fig. 9). This points to pressures below 300 MPa, corresponding to a depth of less than 12 km (NEDELEC & BOUCHEZ, ibidem). The micaceous alteration of the andalusites are explained by late magmatic to subsolidus reactions. The leucogranitic body does not show any sign of metamorphic overprint. The lack of primary contacts and the lack of aureoles within the hosting paragneisses as well as the tectonic contact observed are in favour of a tectonic emplacement of the leucogranite.

However, a petrographically and geochemically comparable lithology is represented by a group of the so-called “orthogneisses”. According to BREITER et al. (2005), these “orthogneisses” are peraluminous. However, their A/CNK-



Text-Fig. 9.
The presence of magmatic andalusite (hatched area) in the Al_2SiO_5 diagram is stable at low pressure. The bold line is the hydrated solidus of granite (adapted and modified from NEDELEC & BOUCHEZ, 2015).

ratio, ranging from 1.14 to 1.40, unambiguously confirms that they are S-type granites (Text-Fig. 4b). For this reason, we put the term orthogneiss used by BREITER et al. (2005) under quotation marks. They are embedded in paragneisses of the Monotonous Series in the Czech part of the Moldanubium and termed as Blaník “orthogneiss[es]”. The following summary is based on BREITER et al. (2005) and RENÉ & FINGER (2016). This group of isolated, generally peraluminous “orthogneiss” bodies, each extending from 1 km to some few km in size, ranges from fine to coarse grained two mica “orthogneisses” to muscovite-tourmaline metagranites. Further accessory minerals are garnet and sillimanite (no andalusite). The two mica “orthogneisses” are enriched in boron with contents ranging between 300 and 1,200 ppm. Four analyses with high boron concentrations from the Blaník “orthogneiss” (BREITER et al., 2005), are plotted together with the analyses from Bernreith (Text-Fig. 4a) and coincide well. A further geochemical similarity between the Bernreith leucogranite and the Blaník “orthogneiss” are the depleted Zr and Th contents. The Bernreith leucogranite displays 24 ppm Zr ($n = 4$) and 0.4 ppm Th ($n = 4$, Tab. 1), whereas the Blaník “orthogneiss” contains 40 ppm Zr and 2.1 ppm Th (RENÉ & FINGER, 2016: Tab. 2, $n = 8$) – both concentrations significantly below the crustal average which is set for Zr at 237 ppm and for Th at 10.3 ppm (WEDEPOHL, 1995) and 193 ppm and 10.5 ppm respectably (RUDNIK & GAO, 2014).

The age of the magmatic precursors of the Blaník “orthogneisses” is still a matter of discussion. Rb-Sr whole rock ages of 489 ± 13 Ma and 459 ± 10 Ma respectively (RAJLICH et al., 1992) as well as a zircon age of 508 ± 7 Ma (VRANA & KRÖNER, 1995) point to an Early Paleozoic age of the Blaník “orthogneiss” group. A fairly well comparable zircon age of 475 ± 1.3 Ma has recently been published for a topaz bearing orthogneiss body within the Monotonous Series (Ostrong Unit) of the Southern Bohemian Massif close to the village Laimbach and termed as “Laimbach Gneiss” (STOCKINGER, 2021). Though the geochemistry of this orthogneiss is somewhat different (no tourma-

line) to the Blaník “orthogneisses”, the similar ages point to contemporaneous magmatic events within the Monotonous Serie. A similar, Early Paleozoic age for the Bernreith leucogranite is therefore also assumed.

Conclusions

The Bernreith leucogranite, embedded within paragneisses of the Monotonous Serie (= Ostrong Unit), is a peraluminous muscovite-tourmaline-andalusite bearing plutonic body with a predominately equigranular texture. It is characterised by an ubiquitous disseminated tourmaline (schorl) mineralisation and, consequently, by a significant boron content (up to 1,300 ppm). The B content is interpreted as heritage from the protolith. An ubiquitous, accessory andalusite mineralisation, interpreted as of magmatic origin, emphasises the peraluminous bulk chemistry of the Bernreith leucogranite. Low K/Rb ratios, a single fluorine content of \approx 2,300 ppm, elevated tin concentrations ranging between 15 and 55 ppm and a maximal Rb content of \approx 430 ppm point to a weak internal differentiation within the granitic body.

A mineralogical difference between the Bernreith leucogranite and the Blaník “orthogneiss” has to be referred to. Whereas the former contains andalusite, contains the latter sillimanite. This might easily be explained by a different local tectonic environment.

The Bernreith leucogranite resembles a group of “orthogneisses” subsumed under the term Blaník “orthogneiss[es]” (BREITER et al., 2005; RENÉ & FINGER, 2016) in the northeaster part of the Moldanubium, Czech Republic. The similarity is emphasised by the bulk chemistry as well as the characteristic presence of tourmaline in both leucogranites.

The textural difference to the Bernreith leucogranite does, however, not seem to be of relevance, as the Blaník “orthogneisses” range texturally between “well foliated” to “coarse grained muscovite-tourmaline metagranite” (BREITER et al., 2005), a termination which could easily be applied to the former as well.

The emplacement of the leucogranite remains an open question as, due to the lack of outcrops, no intrusive contact (if ever one exists) nor any contact phenomenon could have been observed which seems to be in favour of a tectonic emplacement of the granitic body. However, the single tectonic contact observed strikes almost rectangular to the NE-SW orientation of the granitic body and might most likely seen as a local phenomenon.

In any case, the mineralogical and geochemical similarities between the Bernreith leucogranite and the Blaník “orthogneisses” are in favour of grouping them together.

Since the Blaník “orthogneiss[es]” are interpreted as early Paleozoic magmatic intrusions into the Monotonous Series (BREITER et al., 2005; RENÉ & FINGER, 2016), with some restrictions, the Bernreith leucogranite might therefore also be part of this regional event.

Acknowledgements

We would like to thank LUTZ NASDALA, Institute for Mineralogy and Crystallography, Faculty of Earth Sciences, Geography and Astronomy, University of Vienna, for identification of andalusite via Raman spectroscopy and HEINZ REITNER, Geologische Bundesanstalt, Vienna, for drawing the geological map. We also thank FRANZ KIRALY, Department of Lithospheric Research, for the microprobe analyses. We greatly appreciate the editorial handling of CHRISTOPH JANDA that highly improved the quality of this paper.

References

- BREITER, K., ČOPJAKOVÁ, R., GABAŠOVÁ, A. & ŠKODA R. (2005): Chemistry and mineralogy of orthogneisses in the northeastern part of the Moldanubium. – Journal of the Czech Geological Society, **50**/3–4, 81–94, Praha. <https://doi.org/10.3190/JCGS.979>
- BURIANEK, D. & NOVAK, M. (2001): Tourmaline-Bearing Leucogranites from the Moldanubium. – Mitteilungen der Österreichischen Mineralogischen Gesellschaft, **146**, 51–53, Wien.
- BURIANEK, D. & NOVAK, M. (2007): Compositional evolution and Substitution in disseminated tourmaline from leucocratic granites: Examples from the Bohemian Massif, Czech Republic. – Lithos, **95**/1–2, 148–164, Amsterdam. <https://doi.org/10.1016/j.lithos.2006.07.006>
- CLARKE, D.B., DORAIS, M., BARBARIN, B., BARKER, D., CESARE, B., CLARKE, G., EL BAGHDADI, M., ERDMANN, S., FÖRSTER, H.-J., GAETA, M., GOTTESMANN, B., JAMIESON, R.A., KONTAK, D.J., KOLLER, F., LEAL GOMES, C., LONDON, D., MORGAN, G.B. VI, NEVES, L.J.P.F., PATTISON, D.R.M., PEREIRA, A.J.S.C., PICHAVANT, M., RAPELA, C.W., RENNO, A.D., RICHARDS, S., ROBERTS, M., ROTTURA, A., SAAVEDRA, J., NOBREGA SIAL, A., TOSELLI, A.J., UGIDOS, J.M., UHER, P., VIL-LASECA, C., VISONÀ, D., WHITNEY, D.L., WILLIAMSON, B. & WOODARD, H.H. (2005): Occurrence and Origin of Andalusite in Peraluminous Felsic Igneous Rocks. – Journal of Petrology, **46**/3, 441–472, Oxford. <https://doi.org/10.1093/petrology/egh083>
- FUCHS, G. (1979): Bericht 1977 über geologische Aufnahmen im Kristallin auf Blatt 36, Ottenschlag (Waldviertel). – Verhandlungen der Geologischen Bundesanstalt 1978, A51–A54, Wien.
- FUCHS, G. (1983): Bericht 1982 über geologische Aufnahmen auf Blatt 36, Ottenschlag. – Jahrbuch der Geologischen Bundesanstalt, **126**, 299–300, Wien.
- FUCHS, G. & FUCHS, W. (1986): Geologische Karte der Republik Österreich 1:50.000, Blatt 36 Ottenschlag. – 1 Blatt, Geologische Bundesanstalt, Wien.
- FUCHS, G. & ROETZEL, G. (1990): Erläuterungen zu Blatt 36 Ottenschlag. – 64 S., Geologische Bundesanstalt, Wien.
- HAWTHORNE, F.C. & HENRY, D.J. (1999): Classification of the minerals of the tourmaline group. – European Journal of Mineralogy, **11**/2, 201–215, Stuttgart. <https://doi.org/10.1127/ejm/11/2/0201>
- HOLDAWAY, M.J. (1971): Stability of andalusite and the aluminium-silicate phase diagram. – American Journal of Science, **271**, 97–131, Philadelphia. <https://doi.org/10.2475/ajs.271.2.97>
- KLOMÍNSKÝ, J., JARCHOVSKÝ, T. & RAJPOOT, G.S. (2010): Atlas of plutonic rocks and orthogneisses in the Bohemian Massif 2, Moldanubium. – 201 S., Czech Geological Survey, Praha.

- KLÖTZLI, U., FRANK, W., SCHARBERT, S. & THÖNI, M. (1999): Evolution of the SE Bohemian Massif Based on Geochronological Data-A Review. – Jahrbuch der Geologischen Bundesanstalt, **140**/4, 377–394, Wien.
- LINNER, M. (1992): Metamorphose der Paragneise in der Monotonen Serie (SE Moldanubikum). – Dissertation, Universität Wien, 83 + 24 S., Wien.
- LINNER, M. (1996): Metamorphism and partial melting of paragneisses of the Montonous Group, SE Moldanubikum (Austria). – Mineralogy and Petrology, **58**, 215–234, Wien.
- LONDON, D. (1999): Stability of tourmaline in peraluminous granite systems: the boron cycle from anatexis to hydrothermal aureole. – European Journal of Mineralogy, **11**/2, 253–262, Stuttgart.
- MIDDLEMOST, E.A.K. (1994): Naming materials in magma/igneous rock system. – Earth Science Reviews, **37**/3–4, 215–224, Amsterdam. [https://doi.org/10.1016/0012-8252\(94\)90029-9](https://doi.org/10.1016/0012-8252(94)90029-9)
- NEDELEC, A. & BOUCHEZ, J.-L. (2015): Granites – Petrology, Structure, Geological Setting and Metallogeny. – 335 S., Oxford (Oxford University Press).
- PEARCE, J.A., HARRIS, N.B.W. & TINDLE, A.G. (1984): Trace Element Discrimination Diagrams for the Tectonic Interpretation of Granitic Rocks. – Journal of Petrology, **25**/4, 956–983. <https://doi.org/10.1093/petrology/25.4.956>
- PESQUERA, A., TORRES-RUIZ, J., GARCÍA-CASCO, A. & GIL-CRESPO, P.P. (2013): Evaluating the Controls on Tourmaline Formation in Granitic Systems: a Case Study on Peraluminous Granites from the Central Iberian Zone (CIZ), Western Spain. – Journal of Petrology, **54**/3, 609–634, Oxford. <https://doi.org/10.1093/petrology/egs080>
- PETRAKAKIS, K. (1997): Evolution of Moldanubian rocks in Austria: review and synthesis. – Journal of Metamorphic Geology, **15**/2, 203–222, Oxford. <https://doi.org/10.1111/j.1525-1314.1997.00015.x>
- PHILPOTTS, A.R. & AGUE, J.J. (2009): Principles of Igneous and Metamorphic Petrology. – Second edition, 667 S., Cambridge (Cambridge University Press).
- RAJLICH, P., PEUCAT, J.J., KANTOR, J. & RYCHTAŘ, J. (1992): Variscan shearing in the Moldanubian of the Bohemian Massif: deformation, gravity, K-Ar and Rb-Sr data from the Choustník Prevariscan orthogneiss. – Jahrbuch der Geologischen Bundesanstalt, **135**, 579–595, Wien.
- RENÉ, M. & FINGER, F. (2016): The Blaník Gneiss in the Southern Bohemian Massif (Czech Republic): a rare rock composition among the early Palaeozoic granites of the Variscan Central Europe. – Mineralogy and Petrology, **110**, 503–514, Wien.
- RUDNICK, R.L. & GAO, S. (2014): Composition of the Continental Crust. – In: HOLLAND, H.D. & TUREKIAN, K.K. (Eds.): Treatise on Geochemistry (Second Edition), Volume 4: Crust, 1–51, Amsterdam (Elsevier). <https://doi.org/10.1016/B978-0-08-095975-7.00301-6>
- STOCKINGER, V. (2021): Geochronologie, Geochemie und Petrologie eines Topas-führenden Orthogneises innerhalb der „Monotonen Serie“ (Ostrong Einheit, NÖ). – Dissertation, Universität Wien, 80 S., Wien.
- VRANA, S. & KRÖNER, A. (1995): Pb-Pb zircon age for tourmaline alkali-feldspar orthogneiss from Hluboka nad Vltavou in southern Bohemia. – Journal of the Czech Geological Society, **40**, 127–131, Praha.
- WEDEPOHL, K.H. (1995): The composition of the continental crust. – Geochimica et Cosmochimica Acta, **59**/7, 1217–1232, New York. [https://doi.org/10.1016/0016-7037\(95\)00038-2](https://doi.org/10.1016/0016-7037(95)00038-2)
- YAVUZ, F., YAVUZ, V. & SARMAZ, A. (2006): WinClastour – a Visual Basic program for tourmaline formula calculation and classification. – Computers & Geoscience, **32**, 1156–1168, Amsterdam. <https://doi.org/10.1016/j.cageo.2005.10.021>
- ZEUG, M., NASDALA, L., WANTHANACHAISAENG, B., BALMER, W.A., CORFU, F. & WILDNER, M. (2018): Blue zircon from Ratanakiri, Cambodia. – Journal of Gemmology, **36**/2, 112–132, London. <https://doi.org/10.15506/JoG.2018.36.2.112>

Received: 4. May 2022, accepted: 11. July 2023

Appendix

Sample	TU 1		TU 2									
Point	7_1	8_1	20_1	21_1	22_1	23_1	24_1	25_1	26_1	27_1	34_1	35_1
SiO ₂	63.19	64.05	63.40	63.25	62.86	63.81	63.96	63.87	63.75	63.61	63.38	62.51
Al ₂ O ₃	19.07	18.90	19.00	19.27	19.26	18.95	18.96	18.91	19.00	19.14	19.07	19.39
CaO	0.01	0.01	0.01	0.01	0.01	0.01	0.02	0.05	0.03	0.01	0.03	0.02
Na ₂ O	0.46	0.50	0.37	0.50	0.28	0.38	0.58	0.69	0.35	0.39	0.32	0.69
K ₂ O	16.11	16.00	16.14	15.81	16.13	16.03	15.93	15.87	16.21	16.03	16.11	15.65
Total	98.84	99.46	98.92	98.84	98.54	99.18	99.45	99.39	99.34	99.18	98.91	98.26
An	< 0.1	0.10	0.10	0.10	0.10	0.10	0.10	0.10	0.20	0.20	0.10	0.20
Ab	4.20	4.50	3.40	4.60	2.60	3.50	5.20	6.20	3.20	3.60	2.90	6.30
Or	95.80	95.40	96.60	95.40	97.40	96.50	94.70	93.60	96.70	96.40	96.90	93.60

Tab. 2, part 1.
Electron Microprobe Analyses of K-feldspar (wt-%).

Sample	WP-29-1						WP 29-3						
Point	37_1	38_1	39_1	40_1	41_1	15_1	16_1	17_1	30_1	31_1	32_1	33_1	34_1
SiO ₂	62.96	63.68	63.54	64.11	63.84	64.86	64.71	64.86	64.59	64.78	64.95	64.92	64.96
Al ₂ O ₃	18.94	19.00	19.01	19.01	18.70	18.81	18.88	18.93	18.96	18.99	19.15	18.85	18.90
CaO	0.01	0.01	0.01	0.01	0.03	0.01	0.03	0.01	0.01	0.01	0.01	0.01	0.01
Na ₂ O	0.52	0.80	0.53	1.01	0.28	0.71	0.60	1.04	0.85	0.99	0.87	0.92	0.65
K ₂ O	15.90	15.61	15.86	16.21	16.42	15.73	15.72	15.21	15.53	15.26	15.55	15.29	15.78
Total	98.33	99.10	98.95	100.35	99.27	100.12	99.94	100.05	99.94	100.03	100.53	99.99	100.30
An	0.10	< 0.1	0.10	< 0.1	0.10	< 0.1	0.20	< 0.1	< 0.1	0.10	< 0.1	0.10	0.10
Ab	4.70	7.20	4.80	8.60	2.50	6.40	5.50	9.40	7.70	9.00	7.80	8.40	5.90
Or	95.20	92.70	95.10	91.30	97.30	93.50	94.40	90.50	92.30	91.00	92.10	91.60	91.00

Tab. 2, part 2.
Electron Microprobe Analyses of K-feldspar (wt-%).

Sample	TU 2													
Point	1_1	2_1	3_1	4_1	5_1	6_1	7_1	8_1	9_1	10_1	11_1	12_1	28_1	29_1
SiO ₂	67.66	68.70	67.53	64.78	64.75	65.66	64.45	64.70	64.56	65.74	66.26	66.35	65.00	65.98
Al ₂ O ₃	20.52	20.19	20.34	22.08	22.25	21.96	22.08	22.11	22.28	21.61	21.27	21.17	21.87	21.67
CaO	0.90	0.41	0.68	2.43	2.52	2.22	2.43	2.43	2.44	1.74	1.26	1.03	1.96	1.64
K ₂ O	0.06	0.09	0.12	0.14	0.32	0.32	0.15	0.14	0.41	0.35	0.20	0.15	0.20	0.15
Na ₂ O	11.33	11.54	11.40	10.48	10.33	10.43	10.44	10.54	10.20	10.72	10.98	11.15	10.82	11.00
SUM	100.47	100.24	100.07	99.91	100.17	100.59	99.55	99.92	99.89	100.16	99.97	99.85	99.85	100.44
An	4.20	1.90	3.20	11.30	11.70	10.30	11.30	11.20	11.40	8.10	5.90	4.80	9.00	7.50
Ab	95.50	97.60	96.20	88.00	86.60	87.90	87.90	88.00	86.30	90.00	93.00	94.30	89.90	91.60
Or	0.30	0.50	0.70	0.80	1.80	1.80	0.80	0.80	2.30	1.90	1.10	0.80	1.10	0.80

Tab 3, part 1.
Electron Microprobe Analyses of plagioclase (wt-%).

Sample	TU 2			WP 29-1				TU 1			WP 29-3		WP 29-3-A1	
Point	30_1	31_1	33_1	42_1	43_1	44_1	45_1	10_1	12_1	14_1	28_1	29_1	26_1	27_1
SiO ₂	65.85	67.10	67.03	66.32	66.00	66.29	65.38	67.11	67.03	68.09	66.32	66.62	66.51	66.31
Al ₂ O ₃	21.37	20.31	20.51	20.98	21.13	20.55	21.55	21.00	20.39	20.26	21.38	21.62	20.75	20.81
CaO	1.39	0.45	0.53	1.58	1.55	1.37	1.81	1.06	0.61	0.45	1.71	1.75	0.90	0.38
K ₂ O	0.11	0.21	0.18	0.07	0.08	0.05	0.22	0.11	0.15	0.15	0.28	0.24	0.12	0.12
Na ₂ O	11.17	11.66	11.45	11.04	11.05	11.37	10.84	11.21	11.08	11.43	10.50	10.67	11.42	11.46
SUM	99.89	99.73	99.70	99.99	99.81	99.63	99.80	100.49	99.26	100.38	100.19	100.90	99.70	99.08
An	6.40	2.10	2.50	7.30	7.20	6.20	8.30	4.90	2.90	2.10	8.10	8.20	7.96	3.51
Ab	93.00	96.80	96.50	92.30	92.40	93.50	90.40	94.50	96.20	97.10	90.30	90.50	91.41	95.83
Or	0.60	1.10	1.00	0.40	0.40	0.30	1.20	0.60	0.90	0.80	1.60	1.30	0.63	0.66

Tab 3, part 2.
Electron Microprobe Analyses of plagioclase (wt-%).

Sample	TU 1			WP 13				TU 2		WP 29-1				WP 29-3	
Point	4_1	5_1	6_1	8_1	9_1	10_1	11_1	18_1	19_1	46_1	47_1	48_1	49_1	12_1	13_1
SiO ₂	35.64	35.08	35.27	35.68	35.56	35.90	35.43	35.94	34.68	35.84	35.58	35.39	34.81	36.04	35.95
TiO ₂	0.46	0.66	0.82	0.50	0.81	0.21	0.86	0.28	0.94	0.69	0.65	0.77	1.01	0.69	0.80
Al ₂ O ₃	35.19	34.87	35.19	35.31	34.34	35.64	34.50	36.60	35.20	35.68	35.52	35.82	35.62	34.79	34.94
FeO	10.49	10.24	10.38	10.27	10.27	10.21	10.80	10.05	11.22	9.39	9.07	9.17	11.03	9.57	9.17
MnO	0.11	0.12	0.11	0.11	0.18	0.09	0.12	0.10	0.21	0.10	0.10	0.09	0.17	0.10	0.10
MgO	2.44	2.74	2.74	2.54	2.61	2.24	2.48	2.57	2.36	3.71	3.81	3.58	2.45	3.46	3.25
CaO	0.10	0.11	0.14	0.14	0.11	0.06	0.12	0.07	0.16	0.16	0.17	0.15	0.17	0.17	0.16
Na ₂ O	1.52	1.66	1.71	1.72	1.77	1.47	1.71	1.41	1.83	1.82	1.80	1.79	1.75	1.78	1.66
K ₂ O	0.02	0.05	0.04	0.03	0.03	0.02	0.03	0.02	0.03	0.03	0.03	0.04	0.03	0.04	0.03
H ₂ O*	3.19	3.22	3.26	3.26	3.25	3.17	3.24	3.20	3.28	3.34	3.32	3.31	3.28	3.30	3.26
B ₂ O ₃ *	10.52	10.45	10.55	10.56	10.47	10.54	10.48	10.70	10.50	10.73	10.66	10.66	10.57	10.63	10.59
Li ₂ O*	0.08	0.08	0.10	0.15	0.18	0.11	0.13	0.02	0.08	0.07	0.07	0.08	0.06	0.14	0.17
Total	99.75	99.28	100.30	100.27	99.57	99.66	99.90	100.95	100.49	101.56	100.77	100.85	100.95	100.71	100.07

* = calculated after YAVUZ et al. (2006).

Tab. 4a, part 1.

a) Electron Microprobe Analyses of tourmaline (wt-%).

b) Electron Microprobe Analyses of tourmaline (wt-%); profile A–B in sample TU 1 (Text-Figs. 6, 7).

Sample	WP 29-3										WP 29-3_A2			
Point	14_1	24_1	25_1	26_1	27_1	35_1	36_1	37_1	40_1	41_1	42_1	36_1	41_1	42_1
SiO ₂	35.82	35.96	35.50	36.06	35.62	36.35	36.02	36.56	35.84	35.84	35.49	35.85	35.96	35.81
TiO ₂	0.98	0.81	0.93	0.80	0.86	0.65	0.63	0.37	0.82	0.83	0.77	0.88	0.48	0.89
Al ₂ O ₃	35.08	35.52	34.69	35.11	35.31	35.12	34.97	35.72	35.05	34.34	34.48	34.73	35.20	34.74
FeO	9.36	9.03	10.53	9.23	9.52	8.99	9.00	8.81	9.43	9.71	11.26	9.97	11.39	10.69
MnO	0.10	0.12	0.18	0.10	0.10	0.11	0.11	0.11	0.06	0.14	0.15	0.13	0.21	0.18
MgO	3.28	3.31	3.13	3.61	3.37	3.56	3.65	3.33	3.12	3.53	2.47	3.04	1.85	2.46
CaO	0.18	0.20	0.14	0.17	0.17	0.17	0.16	0.08	0.15	0.20	0.17	0.13	0.09	0.15
Na ₂ O	1.69	1.75	1.89	1.76	1.78	1.85	1.73	1.39	1.68	1.87	1.71	1.83	1.68	1.75
K ₂ O	0.04	0.02	0.03	0.03	0.04	0.04	0.04	0.03	0.03	0.05	0.05	0.02	0.10	0.05
H ₂ O*	3.28	3.31	3.32	3.31	3.31	3.34	3.29	3.19	3.26	3.33	3.26	3.30	3.26	3.28
B ₂ O ₃ *	10.63	10.67	10.60	10.68	10.64	10.69	10.62	10.69	10.59	10.58	10.51	10.59	10.58	10.57
Li ₂ O*	0.16	0.19	0.09	0.13	0.12	0.20	0.13	0.08	0.16	0.15	0.10	0.17	0.16	0.18
Total	100.59	100.89	101.03	100.98	100.83	101.07	100.35	100.36	100.19	100.57	100.42	100.64	100.96	100.75

* = calculated after YAVUZ et al. (2006).

Tab. 4a, part 2.

a) Electron Microprobe Analyses of tourmaline (wt-%).

b) Electron Microprobe Analyses of tourmaline (wt-%); profile A–B in sample TU 1 (Text-Figs. 6, 7).

Point	1	2	3	4	5	6	7	8	9	10	11
<hr/>											
SiO ₂	34.60	34.73	34.63	35.17	35.09	35.12	35.18	35.29	35.84	35.99	35.92
TiO ₂	0.39	0.92	0.91	0.83	0.89	0.87	0.86	0.77	0.40	0.28	0.29
Al ₂ O ₃	34.91	34.74	34.97	34.92	34.91	35.09	35.22	35.08	36.03	36.12	36.13
FeO	12.62	11.06	10.79	9.52	9.38	9.20	9.12	9.02	9.12	9.25	9.26
MnO	0.31	0.17	0.14	0.11	0.11	0.09	0.10	0.10	0.10	0.11	0.11
MgO	1.35	2.56	2.63	3.42	3.48	3.68	3.78	3.72	3.13	3.00	3.01
CaO	0.08	0.16	0.15	0.15	0.17	0.19	0.20	0.20	0.08	0.07	0.06
Na ₂ O	1.55	1.75	1.71	1.75	1.79	1.82	1.85	1.82	1.43	1.44	1.39
K ₂ O	0.00	0.00	0.00	0.00	0.00	0.00	0.00	0.00	0.00	0.00	0.00
H ₂ O*	2.93	3.08	3.08	3.10	3.18	3.17	3.18	3.16	3.11	3.12	3.15
B ₂ O ₃ *	10.35	10.45	10.45	10.52	10.52	10.56	10.59	10.56	10.63	10.64	10.63
Li ₂ O*	0.12	0.16	0.15	0.18	0.19	0.18	0.18	0.20	0.19	0.20	0.18
Total	99.19	99.79	99.61	99.68	99.71	99.97	100.26	99.90	100.07	100.21	100.13

* = calculated after YAVUZ et al. (2006).

Tab. 4b, part 1.

a) Electron Microprobe Analyses of tourmaline (wt-%).

b) Electron Microprobe Analyses of tourmaline (wt-%); profile A–B in sample TU 1 (Text-Figs. 6, 7).

Point	12	13	14	15	16	17	18	19	20	21	22
<hr/>											
SiO ₂	35.67	35.88	35.60	35.14	35.21	35.28	35.07	35.07	35.08	35.15	35.16
TiO ₂	0.28	0.28	0.32	0.78	0.82	0.77	0.81	0.82	0.84	0.85	0.88
Al ₂ O ₃	36.03	36.17	36.12	35.26	35.09	35.21	35.07	34.98	35.10	35.13	35.02
FeO	9.32	9.23	9.10	9.37	9.31	9.27	9.35	9.36	9.32	9.14	9.21
MnO	0.11	0.09	0.09	0.10	0.10	0.10	0.10	0.10	0.09	0.11	0.10
MgO	2.99	3.05	3.04	3.60	3.60	3.56	3.57	3.49	3.38	3.51	3.54
CaO	0.06	0.07	0.08	0.18	0.15	0.17	0.17	0.15	0.17	0.16	0.17
Na ₂ O	1.41	1.41	1.45	1.79	1.81	1.76	1.82	1.75	1.79	1.84	1.76
K ₂ O	0.00	0.00	0.00	0.00	0.00	0.00	0.00	0.00	0.00	0.00	0.00
H ₂ O*	3.12	3.15	3.10	3.15	3.13	3.14	3.19	3.11	3.12	3.15	3.13
B ₂ O ₃ *	10.59	10.64	10.59	10.57	10.56	10.57	10.54	10.51	10.52	10.54	10.54
Li ₂ O*	0.17	0.18	0.19	0.16	0.18	0.18	0.17	0.17	0.20	0.21	0.19
Total	99.73	100.16	99.67	100.11	99.95	100.02	99.88	99.50	99.61	99.78	99.69

* = calculated after YAVUZ et al. (2006).

Tab. 4b, part 2.

a) Electron Microprobe Analyses of tourmaline (wt-%).

b) Electron Microprobe Analyses of tourmaline (wt-%); profile A–B in sample TU 1 (Text-Figs. 6, 7).

Sample	TU 1						WP 13			TU 2				
Point	1_1	12_1	3_1	16_1	17_1	18_1	4_1	5_1	6_1	13_1	14_1	15_1	16_1	17_1
SiO ₂	35.76	35.81	35.78	36.00	35.78	36.00	36.27	36.06	36.29	34.88	34.64	34.87	35.47	35.82
TiO ₂	0.06	0.08	0.05	0.05	0.10	0.05	0.16	0.07	0.04	0.08	0.11	0.02	0.08	0.03
Al ₂ O ₃	20.87	20.97	20.98	20.90	20.91	20.86	20.83	20.81	20.81	21.10	21.11	21.13	21.10	21.09
FeO	26.08	25.27	25.74	26.21	25.18	26.16	22.09	22.34	22.14	25.24	25.32	26.05	25.71	26.02
MnO	16.45	16.86	16.59	16.20	17.16	16.08	19.89	19.98	20.13	17.15	17.15	15.98	16.89	16.30
MgO	0.42	0.46	0.41	0.41	0.43	0.36	0.27	0.27	0.25	0.41	0.42	0.34	0.44	0.41
CaO	0.18	0.16	0.17	0.15	0.16	0.13	0.16	0.18	0.25	0.16	0.17	0.11	0.14	0.15
Total	99.82	99.61	99.72	99.92	99.72	99.64	99.67	99.71	99.91	99.02	98.92	98.50	99.83	99.82
Alm	0.596	0.583	0.592	0.602	0.578	0.605	0.515	0.516	0.511	0.579	0.579	0.606	0.587	0.599
Sps	0.382	0.394	0.386	0.377	0.399	0.377	0.469	0.467	0.471	0.399	0.399	0.377	0.391	0.380
Prp	0.017	0.019	0.017	0.017	0.018	0.015	0.011	0.011	0.010	0.017	0.017	0.014	0.018	0.017
Grs	0.001	0.002	0.003	0.003	0.002	0.002	0.000	0.003	0.006	0.001	0.003	0.003	0.001	0.003
Adr	0.004	0.002	0.002	0.002	0.003	0.002	0.005	0.002	0.001	0.004	0.008	0.001	0.003	0.001

Tab. 5.
Electron Microprobe Analyses of garnet (wt-%).

Sample	WP 13				WP 29-3					WP 29-1		WP 29-3_A1	WP 29-3_A2	WP 29-3_A3		
Point	1_1	1_2	18_1	19_1	38_1	39_1	43_1	44_1	2_1	3_1	13_1	14_1	30_1	31_1	43_1	44_1
SiO ₂	36.72	36.58	36.61	36.60	36.61	36.66	36.40	36.62	36.00	36.50	35.46	36.19	35.99	36.65	36.67	36.39
TiO ₂	0.06	0.07	0.06	0.05	0.17	0.18	0.02	0.03	0.09	0.04	0.05	0.04	0.17	0.15	0.03	0.03
Al ₂ O ₃	63.20	62.99	63.14	63.21	62.20	61.92	63.27	62.91	62.61	63.12	63.16	62.67	62.03	62.27	62.97	63.56
FeO	0.19	0.24	0.29	0.26	0.93	0.98	0.17	0.19	0.43	0.19	0.27	0.26	1.00	0.71	0.22	0.19
MnO	< 0.01	< 0.01	< 0.01	< 0.01	< 0.01	< 0.01	< 0.01	< 0.01	< 0.01	0.01	< 0.01	0.01	< 0.01	0.01	< 0.01	0.01
MgO	< 0.01	< 0.01	0.06	0.03	0.14	0.18	0.03	0.02	0.03	0.01	0.02	< 0.01	0.15	0.11	< 0.01	< 0.01
SUM	100.17	99.88	100.16	100.15	100.05	99.92	99.89	99.77	99.07	99.87	98.96	99.17	99.34	99.90	99.89	100.18

Tab. 6.
Electron Microprobe Analyses of andalusite (wt-%).

Sample	WP 29-1		WP 29-3_A1			WP 29-3_A2				WP 29-3_A3					
Point	1_1	4_1	15_1	18_1	59_1	32_1	33_1	34_1	35_1	45_1	46_1	47_1	48_1	49_1	58_1
SiO ₂	31.76	31.27	49.89	50.67	52.67	31.76	52.96	43.53	50.41	45.13	50.79	49.02	49.06	41.16	49.78
Al ₂ O ₃	51.15	51.11	35.27	30.72	28.87	50.72	26.72	41.08	28.98	39.91	33.32	32.92	31.59	44.36	36.18
FeO	0.06	0.15	1.34	1.25	1.25	0.17	1.90	0.29	1.20	0.25	1.16	1.16	1.05	0.20	0.98
MnO	0.02	< 0.01	0.03	0.06	0.09	0.01	0.06	< 0.01	0.05	< 0.01	0.03	0.02	0.03	< 0.01	0.03
MgO	0.01	0.01	1.00	1.81	2.58	0.02	2.70	0.03	2.22	0.04	1.31	1.34	1.63	0.04	0.90
TiO ₂	0.01	0.01	0.03	0.05	0.01	0.05	< 0.01	< 0.01	0.13	< 0.01	0.02	< 0.01	0.01	< 0.01	0.01
Na ₂ O	3.11	0.08	0.17	0.15	0.14	1.45	0.12	0.07	0.14	0.06	0.09	0.07	0.10	0.06	0.09
K ₂ O	0.33	0.24	0.70	0.73	0.60	0.59	0.56	0.28	0.56	0.19	0.42	0.44	0.49	0.27	0.29
SUM	86.45	82.87	88.43	85.44	86.21	84.77	85.02	85.28	83.64	85.58	87.14	84.97	83.96	86.09	88.26

Tab. 7.
Electron Microprobe Analyses of andalusite alteration products (wt-%).

Sample	Matrix mica				mica associated with andalusite									
	WP13		TU1		WP 29-1				WP 29-3_A1					
Point	3_1	7_1	9_1	15_1	5_1	6_1	7_1	8_1	16_1	17_1				
SiO ₂	45.73	45.73	45.43	45.92	45.07	44.69	45.84	44.92	44.12	46.11				
Al ₂ O ₃	35.59	35.71	34.62	35.17	37.48	38.03	36.94	38.45	39.28	36.74				
FeO	0.69	1.48	1.61	1.47	0.37	0.22	0.40	0.14	0.09	0.37				
MnO	na	na	na	na	0.02	0.01	0.05	0.02	0.01	0.03				
MgO	0.20	0.41	0.49	0.47	0.02	0.01	0.04	< 0.01	0.01	< 0.01				
Na ₂ O	0.43	0.54	0.34	0.52	0.29	0.34	0.21	0.40	0.28	0.51				
K ₂ O	11.00	10.60	10.95	10.48	10.96	11.02	10.81	10.96	10.62	10.77				
SUM	93.64	94.47	93.10	94.03	94.21	94.32	94.29	94.89	94.44	94.53				

na = not analysed.

Tab. 8, part 1.
Electron Microprobe Analyses of mica (wt-%).

Sample	mica associated with andalusite									
	WP 29-3_A1				WP 29-3_A2			WP 29-3_A3		
Point	19_1	20_1	21_1	22_1	37_1	38_1	39_1	55_1	56_1	57_1
SiO ₂	32.43	45.71	44.78	44.32	45.01	45.71	45.32	44.33	45.71	45.16
Al ₂ O ₃	50.91	38.11	37.89	37.35	37.05	36.13	36.53	37.06	38.00	38.26
FeO	0.12	0.20	0.23	0.31	0.63	1.10	0.75	0.32	0.21	0.21
MnO	< 0.01	0.01	0.03	0.01	0.03	0.02	0.02	< 0.01	0.01	0.02
MgO	< 0.01	< 0.01	< 0.01	< 0.01	0.14	0.22	0.28	0.02	0.01	< 0.01
Na ₂ O	0.48	0.52	0.43	0.37	0.50	0.75	0.40	0.40	0.40	0.37
K ₂ O	1.07	10.58	10.60	10.70	10.62	10.17	10.71	10.86	10.76	10.74
SUM	85.01	95.14	93.97	93.11	93.98	94.64	94.02	93.01	95.10	94.78

Tab. 8, part 2.
Electron Microprobe Analyses of mica (wt-%).